ZnSe–Si Bi-coaxial Nanowire Heterostructures**

By *Chunrui Wang*,* *Juan Wang*, *Quan Li*, and *Gyu-Chul Yi*

We report on the fabrication, structural characterization, and luminescence properties of ZnSe/Si bi-coaxial nanowire heterostructures. Uniform ZnSe/Si bi-coaxial nanowire heterostructures are grown on silicon substrates by the simple one-step thermal evaporation of ZnSe powder in the presence of hydrogen. Both ZnSe and silicon are single-crystalline in the bi-coaxial nanowire heterostructures, and there is a sharp interface along the nanowire axial direction. Furthermore, secondary nanostructures of either ZnSe nanobrushes or a SiO_x sheath are also grown on the primary bi-coaxial nanowires, depending on the ratio of the source materials. The experimental evidence strongly suggests that bi-coaxial nanowires are formed via a co-growth mechanism, that is, ZnSe terminates specific surfaces of silicon and leads to anisotropic, one-dimensional silicon growth, which simultaneously serves as preferential nucleation sites for ZnSe, resulting in the bi-coaxial nanowire heterostructures. In addition, the optical properties of ZnSe/Si nanowires are investigated using low-temperature photoluminescence spectroscopy.

1. Introduction

One-dimensional (1D) semiconductor nanostructures have attracted considerable research attention because of their great potential for fundamental research on the effect of dimensionality and size on physical properties, as well as for electronic and optoelectronic nanodevice applications.[1] In recent years, various methods,[2] including laser-assisted catalytic growth, chemical vapor deposition, metal–organic chemical vapor deposition (MOCVD), and thermal evaporation have been developed to fabricate 1D semiconductor heterostructures, such as GaAs/GaP,[2a] Si/SiGe,[2b] InAs/InP,[2c–e] $ZnO/Zn_{0.8}Mg_{0.2}O$,[2f] TiO_2/SnO_2,[2g] Si/Ge,[2h] NiSi/Si,[2i] and GaN/ZnO.[2j,k] The formation of 1D heterostructures is also believed to be of importance in tailoring the physical properties of 1D nanostructures.[2] For example, resonant tunneling and single-electron tunneling behaviors were observed from InAs/InP nanowire heterostructures.[2c] A quantum-confinement effect is present in $ZnO/Zn_{0.8}Mg_{0.2}O$ nanorod heterostructures, where the thickness was controlled precisely, down to the monolayer level.[2f] Heterostructures with various compositions and interfaces have already demonstrated distinctive performances in nanodevice applications.[2c]

ZnSe, which has a well-known wide, direct bandgap (bulk crystal $E_g = 2.7$ eV at 300 K),[3] is potentially a good material for short-wavelength optoelectronic devices, including blue laser diodes (LDs), light-emitting diodes (LEDs), and photodetectors.[4–6] ZnSe-based microstructures have been widely investigated for their potential optoelectronic applications, including high-density optical storage and full-color displays.[7–9] Controlling the size and dimensions of ZnSe may lead to further novel properties.[10] Inspired by this, various 1D forms of ZnSe nanowires (nanorods) and nanoribbons have recently been fabricated.[11] 1D silicon nanowires in particular are very attractive, given their key role in the semiconductor industry and hence the existing set of known fabrication technologies.[12] It is known that single-crystalline silicon nanowires can be readily grown by the disproportionation of SiO powder at elevated temperature.[13] Nanometer-scale, 1D, silicon-based heterostructures are of general interest. Disproportionation, using silicon nanowires as templates, may result in the formation of various 1D, silicon-based heterostructures.[2h,l] Nevertheless, multistep deposition, involving a change of the source materials or the reactor temperature, is usually troublesome. Recently, Si–ZnS and Si–ZnSe biaxial nanowires and ZnS–Si–ZnS triaxial nanowires were fabricated by Hu et al. via the two-stage thermal evaporation of mixed SiO and ZnS or SiO and ZnSe powders.[2l] Those nanostructures are expected to open a new field of Group II–VI/Si-based nano-heterostructure research.

In our previous study, we demonstrated that Si-core/CdSe-sheath nanocables could be synthesized in a silicon substrate via the thermal evaporation of CdSe.[14] However, an amorphous layer was present at the silicon–CdSe interface. Herein,

[*] Prof. C. R. Wang
Department of Physics, Donghua University
Shanghai 200051 (P.R. China)
E-mail: wangcr2001@hotmail.com
Prof. C. R. Wang
Department of Physics, Huaibei Coal Industry Teacher's College
Huaibei 235000 (P.R. China)
J. Wang, Prof. Q. Li
Department of Physics, and Chinese University of Hong Kong
Hong Kong (P.R. China)
Prof. G.-C. Yi
National CRI Center for Semiconductor Nanorods and Department of Materials Science and Engineering
Pohang University of Science and Technology (POSTECH)
Pohang, 790-784 (Korea)

[**] This work was supported by The National Natural Science Foundation of China and Anhui Education Department, P.R. China (No. 2005KJ035ZD). We also acknowledge the KOSEF for partial financial support. G.-C. Yi was supported by the National Creative Research Initiative Project of the Ministry of Science and Technology, Korea.

 DOI: 10.1002/adfm.200400564

we report a modification of this method; evaporating ZnSe in the presence of H_2, which results in ZnSe/Si bi-coaxal nanowire heterostructures, with an abrupt interface between the two nanomaterials (along the axial direction) directly growing on silicon substrates. By controlling the weight of ZnSe source material, we observed the secondary growth of ZnSe nanobranches on the primary bi-coaxial nanowire (with excess ZnSe)—resulting in ZnSe nanobrushes; and an amorphous SiO_x sheath outside the bi-coaxial nanowire (with a ZnSe deficiency)—resulting in (ZnSe/Si)-core/SiO_x-sheath nanocables. Furthermore, we have proposed a growth model for the formation of nanowire heterostructures.

2. Results and Discussion

2.1. ZnSe/Si Bi-coaxial Nanowire Heterostructures

Figure 1a is a scanning electron microscopy (SEM) image of as-grown ZnSe/Si bi-coaxial nanowire heterostructures, showing good uniformity and wire-like morphology. These nanowire heterostructures have diameters of less than 100 nm and lengths of several tens of micrometers.

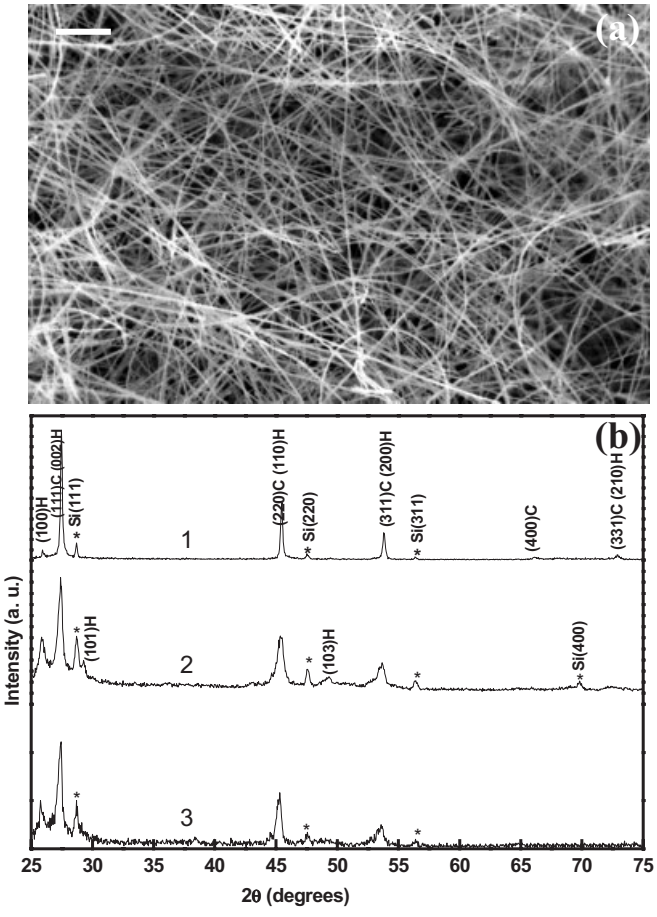

Figure 1. a) SEM image of as-synthesized nanowires (sample 1), scale bar: 1 μm. b) XRD patterns of samples 1–3, respectively, which indicate the existence of cubic silicon and ZnSe (both hexagonal, H, and cubic, C).

The crystal structure of the nanowire heterostructures was investigated using X-ray diffraction (XRD), as shown in Figure 1b. All the diffraction peaks are indexed to cubic silicon and ZnSe (both hexagonal and cubic) within experimental error, indicating that the as-grown nanomaterial is composed of silicon and ZnSe. No characteristic peaks from other crystalline forms were detected in the XRD pattern. The SEM and XRD results demonstrate that the as-grown product is a composite material of ZnSe and silicon with wire-like morphology.

Detailed microstructures of the as-grown nanowires were further investigated using transmission electron microscopy (TEM) and selected-area electron diffraction (SAED). Figure 2a shows a low-magnification TEM image of typical ZnSe/Si nanowire heterostructures prepared by the one-step thermal evaporation of ZnSe (sample 1). The light–dark contrast along the nanowire radial direction indicates its bi-coaxial nature. Each bi-coaxial nanowire heterostructure shows a uniform diameter along its whole length. The typical diameter of these bi-coaxial nanowires is 80–100 nm, and the diameters of the silicon sub-nanowires and ZnSe sub-nanowires range from 30 to 40 nm and 60 to 70 nm, respectively. Two sets of diffraction spots were observed in the SAED pattern taken from individual nanowire heterostructures. One set comes from cubic silicon, and the others can be indexed to either hexagonal ZnSe (*h*-ZnSe; Fig. 2b) or cubic ZnSe (*c*-ZnSe; Fig. 2d), for different nanowires. It is also notable that the *h*- and *c*-ZnSe sub-nanowires prefer to grow along their [002] and [11$\bar{2}$] crystalline directions, respectively, whereas silicon sub-nanowires normally grow along their [11$\bar{2}$] crystalline direction.

High-resolution TEM (HRTEM) images clearly show crystal structures at the ZnSe/Si interfaces of the corresponding nanowires (Figs. 2c,e). In the nanowires examined, both ZnSe and silicon in bi-coaxial nanowire heterostructures were single-crystalline. A clean and abrupt interface between silicon and ZnSe was observed, regardless of whether ZnSe is hexagonal (Fig. 2c) or cubic (Fig. 2e). The bicrystalline nature of the nanowire was further clarified by a cross-sectional TEM image (Fig. 2f) and its corresponding elemental maps (Figs. 2g–i), which were measured at the Si K (1839 eV), Zn L (1020 eV), and Se L edges (1436 eV), respectively. The bi-coaxial nanowire heterostructure has a circular cross-section, with a sharp interface between the silicon and the ZnSe. Unlike the report of Hu et al.[21] and our previous work,[14] no intermediate layer or amorphous layer was observed at the ZnSe/Si interface. The elemental mapping from the cross-section of the bi-coaxial nanowire heterostructure also demonstrates that the bi-coaxial ZnSe/Si has a well-defined radial compositional profile.

Energy-dispersive X-ray analysis (EDX) spectra taken from the light and dark regions also suggest that they are composed of silicon and ZnSe (the copper signal comes from the TEM grid), respectively, which is consistent with the XRD results, as shown in Figure 3. The trace amount of oxygen originates from unavoidable oxygen adsorption on the surface due to exposure to air during sample processing.[21]

ADVANCED FUNCTIONAL MATERIALS

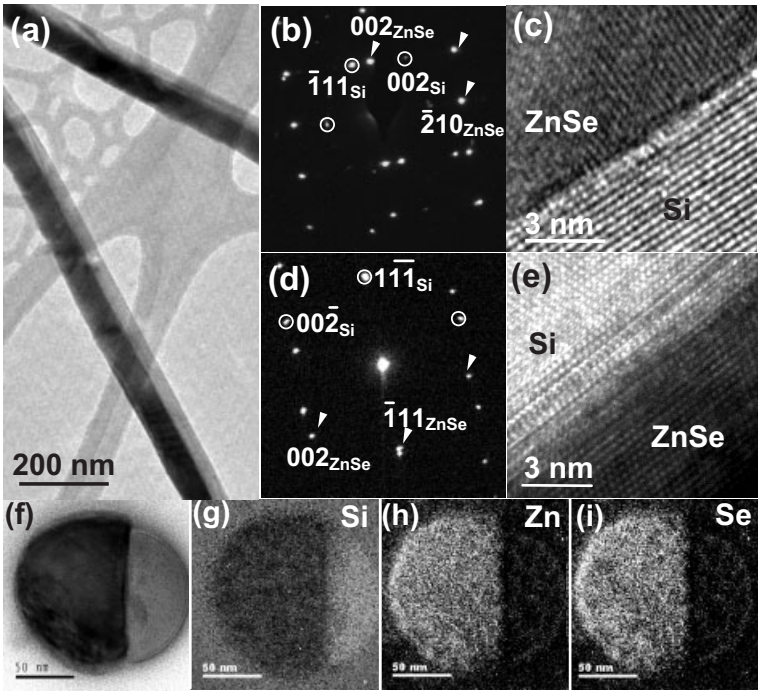

Figure 2. a) TEM image of typical nanowires from sample 1. b) SAED pattern of a single nanowire, which can be indexed to Si<110> and *h*-ZnSe<120> zone axes. c) HRTEM image taken at the ZnSe/Si interface corresponding to Fig. 2b. d) SAED pattern taken from another nanowire, which can be indexed to Si<110> and the *c*-ZnSe<110> zone axes. e) HRTEM image corresponding to Fig. 2d, showing the twin boundary (interface) between silicon and ZnSe. f) TEM image of the cross-section of the bicrystalline nanowire. g–i) Corresponding elemental maps of silicon, zinc and selenium, performed using the Si K (1839 eV), Zn L (1020 eV), and Se L edges (1436 eV), respectively.

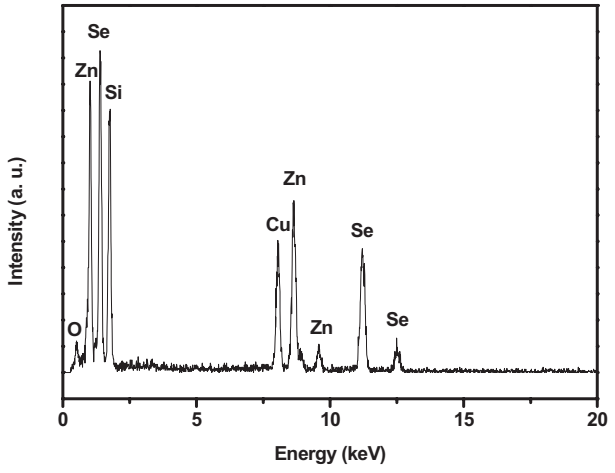

Figure 3. EDX spectrum taken of the individual bicrystalline nanowire heterostructure shown in Figure 2a. The trace amount of oxygen possibly originates from unavoidable oxygen adsorption due to exposure to air during sample processing.

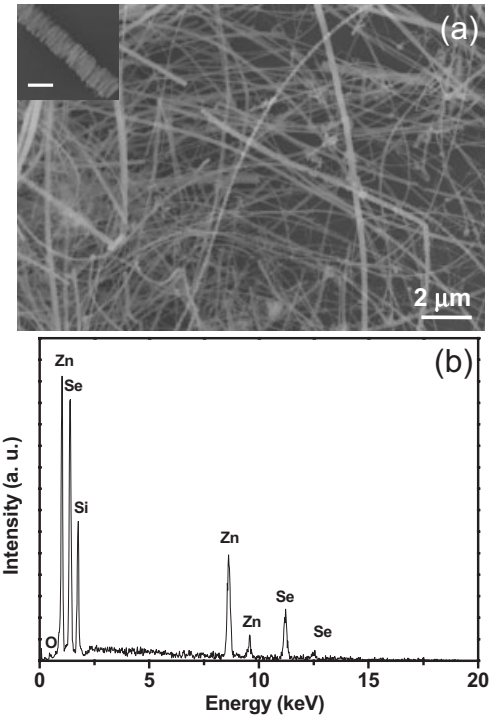

Figure 4. a) SEM image of sample 2. Inset: a high-magnification SEM image depicting nanobranches with diameters of ≈30 nm grown on the nanowire, scale bar: 200 nm. b) EDX spectrum of sample 2 shown in (a).

2.2. Secondary Growth of Nanostructures on ZnSe/Si Bi-coaxial Nanowire Heterostructures

2.2.1. ZnSe Nanobranches Grown on ZnSe/Si Bi-Coaxial Nanowire Heterostructures

A similar one-step evaporation approach was used to grow ZnSe nanobranches on ZnSe/Si bi-coxial nanowires (sample 2), except that an excess of ZnSe source material (in comparison with that of sample 1) was used. Although EDX (Fig. 4b) and XRD (Fig. 1c) results suggest that the chemical composition and crystallinity of sample 2 are similar to those of sample 1, that is, sample 2 is also a composite material of silicon and ZnSe, their morphology differs tremendously, as shown in Figure 4a. The SEM image in the inset of Figure 4a shows as-grown nanomaterial with a comb-like (or brush-like)

morphology, that is, many nanobranches have grown perpendicularly out of a long nanowire.

Figures 5a,b show TEM images of the nanobranches on a nanowire. The TEM images reveal the formation of numerous nanobranches grown on the bi-coaxial nanowire heterostructures with relatively uniform diameters (about 30 nm). If the electron beam is parallel to the bi-coaxial nanowire interface, heterostructures like those shown in Figure 5b are formed; otherwise, heterostructures like those shown in Figure 5a are formed. The SAED pattern (Fig. 5c) taken from an individual nanowire (marked in Fig. 5b) is similar to that of sample 1, that is, two sets of well-correlated diffraction spots corresponding to silicon and ZnSe, respectively. The HRTEM image shown in Figure 5d confirms that these nanobranches are ZnSe with the same crystalline orientation as the ZnSe sub-nanowires in the primary bi-coaxial nanowires.

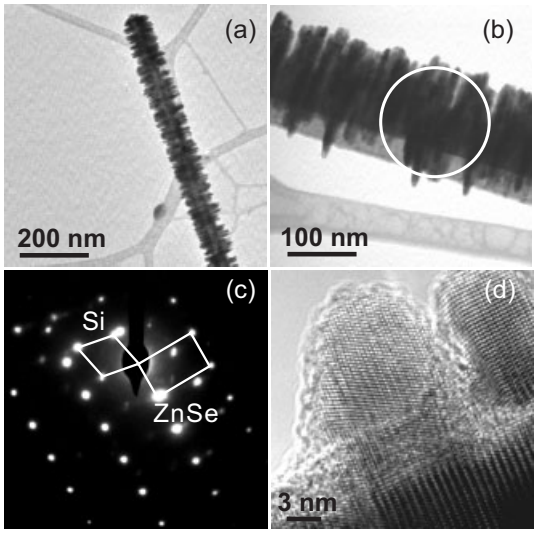

Figure 5. a,b) TEM images of sample 2, revealing nanobranches grown on the bicrystalline nanowire. c) SAED pattern taken from the nanowire marked in (b), which can be indexed to Si<110> and the *h*-ZnSe<120> zone. d) HRTEM image of the nanobranches.

"Comb-like" ZnO structures were observed by Hashimoto and Yamaguchi,[15] but the mechanism that drives their growth was not elaborated until recently.[16] The positively charged Zn(0001) surface is chemically active and the negatively charged O(0001) surface is relatively inert, resulting in the growth of long fingers along [0001].[16] Anisotropic growth appears to be a common characteristic for the wurtzite family. Similar saw-tooth (or comb-like) growth has been observed for ZnS[17] and CdSe,[18] and is suggested to be induced by the Zn- and Cd-terminated (0001) surfaces, respectively.[16]

2.2.2. *ZnSe/Si-Core/SiO_x-Sheath Nanocables*

Different nanostructures were fabricated by using less ZnSe source material than for the growth of sample 1, while keeping the other experimental conditions identical. Figure 1d shows the XRD pattern of the as-grown product (sample 3), indicating the same XRD peak positions as those in samples 1 and 2.

The morphology of sample 3 was also similar to that of sample 1. As shown in Figure 6a, however, TEM images of the individual nanowires exhibited light–dark contrast corresponding to the core–sheath region of an individual nanowire heterostructure.[14] The core was similar to the ZnSe/Si bi-coxial structure of sample 1 with a diameter of 100 nm. A 25 nm amorphous sheath was observed outside the bi-coaxial nanowire core.

The spatial distribution of different compositional elements was also clarified by elemental mapping (Figs. 6c–f), which was performed using the O K (532 eV), Si K (1839 eV), Zn L (1020 eV), and Se L edges (1436 eV), respectively. Zinc and selenium are located in the core region, and silicon in the core and sheath region. The oxygen signal was located in the sheath region. The oxygen and silicon content was much higher in sample 3 (core–sheath structures) than in samples 1 (bi-coaxial nanowires) and 2 (nanobrushes). EDX data (Fig. 7) reveal that the sheath is composed of silicon and oxygen, and the core is a

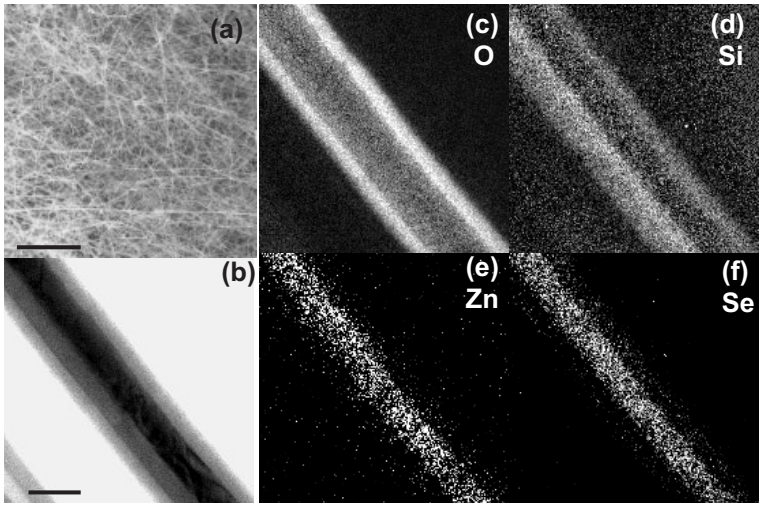

Figure 6. a) SEM image of as-prepared sample 3, scale bar: 1 μm. b) TEM image of a (ZnSe/Si)-core/SiO_x-sheath nanocable (sample 3), scale bar: 100 nm. c–f) Elemental maps of oxygen, silicon, zinc, and selenium, taken at the O K (532 eV), Si K (1839eV), Zn L (1020 eV), and Se L edges (1436 eV), respectively.

ADVANCED FUNCTIONAL MATERIALS

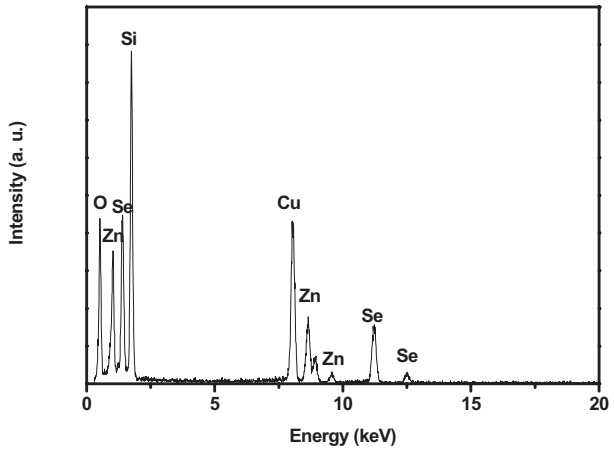

Figure 7. EDX spectrum of the (ZnSe/Si)-core/SiO_x-sheath nanocable shown in Figure 6b. The oxygen and silicon contents in the (ZnSe/Si)-core/SiO_x-sheath nanocable are much higher than those in samples 1 and 2.

composite material of silicon and ZnSe, which is consistent with the structural analysis shown in Figure 6b. The oxygen, silicon, zinc, and selenium elemental mappings from this core–sheath structure (Fig. 6c–f) further demonstrate that ZnSe/Si bi-coaxial nanowire structures have a well-defined compositional profile and an abrupt interface.

2.3. Growth Mechanism

The experimental results suggest that these ZnSe/Si bi-coaxial nanowire heterostructures are grown via a co-growth vapor-transfer mechanism, that is, ZnSe in the vapor phase, which is transferred to the lower temperature zone, in which silicon simultaneously presents and condenses together to form the specific bi-coaxial configuration. In detail: the 1D growth of silicon in the bi-coaxial nanowires is governed by a physical principle similar to the oxide-assisted mechanism where the silicon source (silicon substrates)[14] is provided by the disproportionation reaction of silicon oxide.[13a,19] However, unlike oxide-assisted silicon nanowire growth, it is not the oxygen that terminates specific surfaces of silicon and determines the specific anisotropic silicon nanowire growth (usually with a growth direction along the silicon [11$\bar{2}$] crystalline direction).[20] Instead, ZnSe in the vapor phase plays an important role, as supported by several observations: 1) zinc and selenium present at the ZnSe/Si interface (Figs. 2g–i), which terminate the specific surfaces of silicon; 2) silicon sub-nanowires in bi-coaxial nanowires usually grow along their [11$\bar{2}$] crystalline direction (Fig. 2c,e); 3) the presence of hydrogen is important, as it effectively decreases the oxygen concentration in the gas atmosphere, otherwise an amorphous oxide layer is present at the interface of the wires.[14] Once the specific surfaces of silicon are terminated, the ZnSe serves as preferential sites for homophase nucleation, resulting in ZnSe/Si bi-coaxial nanowires.

The specific cross-sectional configuration of bi-coaxial nanowire heterostructures (Fig. 2f) may be caused by a thermodynamic factor—the bi-coaxial nanowire grows in a way that minimizes its interfacial energy.[21] Both hexagonal (metastable) and cubic (stable) ZnSe phases are present, presumably owing to the high deposition temperature[22] and the deposition process which deviated from thermal equilibrium. The lack of orientation relation between *h*-ZnSe and silicon may be explained in terms of the large lattice mismatch and the different crystalline symmetry between the two materials.

The co-growth mechanism is further supported by experimental observations from samples 2 and 3. When there is either an excess or deficiency of source material, the co-growth process is terminated, and secondary growth of the extra ZnSe (or SiO_x) starts on the primary bi-coaxial nanowires. The formation of extra ZnSe nanobranches only on the ZnSe sub-nanowires of the bi-coaxial nanowire may result from the anisotropic crystal structure of ZnSe. In comparison, the SiO_x that forms a uniform sheath outside the bi-coaxial nanowire may result from its isotropic nature.

In addition, the co-growth mechanism is supported by another experimental fact. While maintaining identical experimental conditions, we only obtained amorphous SiO_x nanowires on silicon substrates in the absence of ZnSe source material, which is similar to the case of SiO_2 nanowires via thermal oxidation of silicon wafers.[23]

2.4. Photoluminescence

Figure 8 shows the 10 K photoluminescence (PL) spectra of the as-grown sample 1 (ZnSe/Si bi-coaxial nanowire heterostructures). The strong peak at 1.766 eV and the weak peak at 1.822 eV presumably result from silicon sub-nanowire emissions. A peak has been observed in a similar position in the PL spectra of luminescent porous silicon,[24a,b] silicon nanowires,[24c] and Si–ZnS biaxial nanowires.[21] The origin of these emissions has been interpreted as arising from free-standing

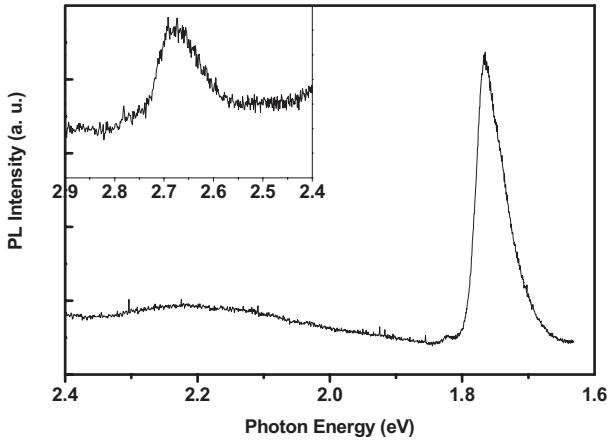

Figure 8. PL spectra of the ZnSe/Si bicrystalline nanowire heterostructures shown in Figure 1a measured at 10 K with the 442 nm line of a He–Cd laser as the optical excitation source. The inset shows a PL spectrum measured on the same specimen at 10 K excited by the 325 nm He–Cd laser line.

silicon nanowires wherein two-dimensional quantum confinement of charge carriers has appreciably widened the silicon bandgap.[24a] The wide band range from 1.999 to 2.350 eV may involve deep-level emission from ZnSe sub-nanowires.[25] This wide band was also observed in the PL spectra of ZnSe nanowires and nanobelts.[1d,11g] The weak peak at 2.782 eV in the inset of Figure 8 is attributed to deep, donor-bound excitons (I_1) in ZnSe sub-nanowires,[26–28] the same peak positions were observed in the PL spectra of ZnSe nanowires and nanobelts.[1d,11g] The 2.694 and 2.665 eV peaks are attributed to donor–acceptor pair recombination (DAP) with a zero-phonon peak and the first phonon replica in ZnSe sub-nanowires, respectively, due to the LO-phonon (LO: longitudinal optical) energy of ZnSe, $\hbar\omega_{LO} = 32 \pm 0.1$ meV.[28]

3. Conclusions

ZnSe/Si bi-coaxial nanowire heterostructures and their secondary nanostructures were grown on silicon substrates by simple thermal evaporation. The bi-coaxial nanowire heterostructures exhibited a clean interface between ZnSe and silicon. Both I_1 and DAP of the ZnSe sub-nanowires and a strong emission of the silicon sub-nanowires were observed in the low-temperature PL spectra of ZnSe/Si bi-coaxial nanowire heterostructures. Furthermore, we have proposed a growth model for the formation of nanowire heterostructures. The design, synthesis, and characterization of nanowire heterostructures or hierarchical structures is of fundamental importance in controlling the mesoscopic properties of new materials and developing new nanofabrication tools.

4. Experimental

The ZnSe/Si nanowire heterostructures were grown using a high-temperature vacuum-tube furnace, as described in detail elsewhere [29]. Briefly, ZnSe (99.99 %, Sigma-Aldrich; 2 g) powder was placed on an alumina boat in the center region of an alumina tube; silicon substrates were placed in downstream in the tube. The tube was then pumped down to a base pressure of 2×10^{-2} torr (1 torr $\approx$ 133 Pa). Argon gas containing 5 % H_2 was introduced into the tube at a constant flow rate of 50 sccm (sccm: standard cubic centimeters per minute). The total pressure was kept at 300 torr during the fabrication process. The furnace was maintained at 1250 °C for two hours before it was cooled to room temperature. A series of samples was fabricated by changing the weight of ZnSe used. Three representative samples (1, 2, and 3) were prepared by thermal evaporation of 2, 3, and 0.5 g ZnSe, respectively: all other experimental conditions were identical.

The structural properties of nanowire heterostructures were investigated using XRD (Rigakau RU-300 with microns Cu Kα_1 radiation), SEM (LEO 1450VP) equipped with EDX, and TEM (Tecnai 20, 200kV, FEG) with a Gatan image filtering (GIF) system attached. Two different types of samples were prepared for the TEM characterization: one was a regular sample, prepared by conventional dispersion, followed by carbon film fishing; the other was a cross-sectional sample. Sample preparation details can be found elsewhere [30]. PL spectroscopy was performed using the 325 or 442 nm line of the He–Cd laser. Details of the PL measurements have been described elsewhere [31].

Received: December 3, 2004
Final version: April 14, 2005

[1] a) X. F. Duan, Y. Huang, Y. Cui, J. Wang, C. M. Lieber, *Nature* **2001**, *409*, 66. b) J. C. Johnson, H. J. Choi, K. P. Knutsen, R. D. Schaller, P. D. Yang, R. J. Saykally, *Nat. Mater.* **2002**, *1*, 106. c) Y. N. Xia, P. D. Yang, Y. G. Sun, Y. Y. Wu, B. Mayers, B. Gates, Y. D. Yin, F. Kim, H. Q. Yan, *Adv. Mater.* **2003**, *15*, 353.

[2] a) M. S. Gudiksen, L. J. Lauhon, J. Wang, D. C. Smoth, C. M. Lieber, *Nature* **2002**, *415*, 617. b) Y. Wu, R. Fan, P. D. Yang, *Nano Lett.* **2002**, *2*, 83. c) B. T. Björk, B. J. Ohlsson, T. Sass, A. I. Persson, C. Thelander, M. H. Magnusson, K. Deppert, L. R. Wallenberg, L. Samuelson, *Appl. Phys. Lett.* **2002**, *80*, 1058. d) B. T. Björk, B. J. Ohlsson, C. Thelander, A. I. Persson, K. Deppert, L. R. Wallenberg, L. Samuelson, *Appl. Phys. Lett.* **2002**, *81*, 4458. e) C. Thelander, M. H. Magnusson, B. T. Björk, B. J. Ohlsson, M. W. Larsson, L. R. Wallenberg, L. Samuelson, *Appl. Phys. Lett.* **2003**, *83*, 2052. f) W. I. Park, G. C. Yi, M. Y. Lim, S. J. Pennycook, *Adv. Mater.* **2003**, *15*, 526. g) R. He, M. Law, F. Kim, D. P. Yang, *Nano Lett.* **2002**, *2*, 1109. h) L. J. Lauhon, M. S. Gudiksen, D. L. Wang, C. M. Lieber, *Nature* **2002**, *420*, 57. i) Y. Wu, J. Xiang, C. Yang, W. Lu, C. M. Lieber, *Nature* **2004**, *430*, 61. j) S. J. An, W. I. Park, G. C. Yi, Y. J. Kim, H. B. Kang, M. Y. Kim, *Appl. Phys. Lett.* **2004**, *84*, 3612. k) J. Goldberger, R. R. He, Y. F. Zhang, S. W. Lee, H. Q. Yan, H. J. Choi, P. D. Yang, *Nature* **2003**, *422*, 599. l) J. Hu, Y. Bando, Z. Liu, T. Sekiguchi, D. Golberg, J. Zhan, *J. Am. Chem. Soc.* **2003**, *125*, 11 306.

[3] R. Rujkorakarn, A. J. Nelson, *J. Appl. Phys.* **2000**, *87*, 8557.

[4] T. Matasuoka, *Adv. Mater.* **1996**, *8*, 469.

[5] R. Pässler, E. Griebl, H. Ripel, G. Lautner, S. Bauer, H. Preis, W. Gebhardt, B. Buda, D. J. As, D. Schikora, K. Lischka, K. Papagelis, S. Ves, *J. Appl. Phys.* **1999**, *86*, 4403.

[6] J. Wang, D. C. Hutchings, A. Miller, E. W. Vanstryland, K. R. Welford, I. T. Muirhead, K. L. Lewis, *J. Appl. Phys.* **1993**, *73*, 4746.

[7] S. K. Hong, E. Kurts, J. H. Chang, T. Hanada, M. Oku, T. Yao, *Appl. Phys. Lett.* **2001**, *78*, 165.

[8] M. A. Haase, J. Qiu, J. M. Depuydt, H. Cheng, *Appl. Phys. Lett.* **1991**, *59*, 1272.

[9] H. Jeon, J. Ding, W. Patterson, A. V. Nurmikko, W. Xie, D. C. Grillo, M. Kobayashi, R. L. Gunshor, *Appl. Phys. Lett.* **1991**, *59*, 3619.

[10] C. M. Lieber, *Nano Lett.* **2002**, *2*, 82.

[11] a) Y. F. Chan, X. F. Duan, S. K. Chan, I. K. Sou, X. X. Zhang, N. Wang, *Appl. Phys. Lett.* **2003**, *83*, 2665. b) Y. Jiang, X. M. Meng, W. C. Yiu, J. Liu, J. X. Ding, C. S. Lee, S. T. Lee, *J. Phys. Chem. B* **2004**, *108*, 2784. c) X. T. Zhang, Z. Liu, K. M. Ip, Y. P. Leung, Q. Li, S. K. Hark, *J. Appl. Phys.* **2004**, *95*, 5752. d) Q. Li, X. Gong, C. R. Wang, J. Wang, K. Ip, S. K. Hark, *Adv. Mater.* **2004**, *16*, 1436. e) B. Xiang, H. Z. Zhang, G. H. Li, F. H. Yang, F. H. Su, R. M. Wang, J. Xu, G. W. Lu, X. S. Sun, Q. Zhao, D. P. Yu, *Appl. Phys. Lett.* **2003**, *82*, 3330. f) Y. C. Zhu, Y. Bando, *Chem. Phys. Lett.* **2003**, *377*, 367. g) X. T. Zhang, K. M. Ip, Z. Liu, Y. P. Leung, Q. Li, S. K. Hark, *Appl. Phys. Lett.* **2004**, *84*, 2641.

[12] D. Ma, C. S. Lee, F. C. Au, S. Y. Tong, S. T. Lee, *Science* **2003**, *299*, 1874.

[13] a) N. Wang, Y. H. Tang, Y. F. Zhang, C. S. Lee, S. T. Lee, *Phys. Rev. B* **1998**, *58*, R16024. b) S. T. Lee, Y. F. Zhang, N. Wang, Y. H. Tang, I. Bello, C. S. Lee, *J. Mater. Res.* **1999**, *14*, 4503. c) W. S. Shi, H. Y. Peng, L. Xu, N. Wang, Y. H. Tang, S. T. Lee, *Adv. Mater.* **2000**, *12*, 1927.

[14] Q. Li, C. R. Wang, *J. Am. Chem. Soc.* **2003**, *125*, 9892.

[15] S. Hashimoto, A. Yamaguchi, *J. Am. Ceram. Soc.* **1996**, *79*, 1121.

[16] Z. L. Wang, X. Y. Kong, Y. Ding, P. X. Gao, W. L. Hughes. R. S. Yang, Y. Zhang, *Adv. Funct. Mater.* **2004**, *14*, 943.

[17] D. Moore, C. Ronning, C. Ma, Z. L. Wang, *Chem. Phys. Lett.* **2004**, *385*, 8.

[18] C. Ma, Y. Ding, D. Moore, X. D. Wang, Z. L. Wang, *J. Am. Chem. Soc.* **2004**, *126*, 708.

[19] N. Wang, Y. F. Zhang, Y. H. Tang, C. S. Lee, S. T. Lee, *Appl. Phys. Lett*. **1998**, *73*, 3902.

[20] S. T. Lee, N. Wang, Y. F. Zhang, Y. H. Tang, *MRS Bull.* **1999**, *24*, 36.

ADVANCED FUNCTIONAL MATERIALS

[21] B. Lewis, J. C. Anderson, *Nucleation and Growth of Thin Films*, Academic Press, New York **1970**.
[22] J. W. Mullin, *Crystallization*, Butterworth–Heinemann, Oxford, UK **1997**.
[23] J. Q. Hu, Y. Jiang, X. M. Meng, C. S. Lee, S. T. Lee, *Chem. Phys. Lett.* **2003**, *367*, 339.
[24] a) L. T. Canham, *Appl. Phys. Lett.* **1990**, *57*, 1046. b) A. G. Cullis, L. T. Canham, *Nature* **1991**, *353*, 335. c) Y. F. Zhang, Y. H. Tang, H. Y. Peng, N. Wang, C. S. Lee, I. Bello, S. T. Lee, *Appl. Phys. Lett.* **1999**, *75*, 1842.
[25] a) R. M. Park, H. A. Mar, N. M. Salansky, *J. Appl. Phys.* **1985**, *58*, 1047. b) T. Yao, Y. Makita, S. Maekawa, *Appl. Phys. Lett.* **1979**, *35*, 97.
[26] K. Mochizuki, K. Masumoto, T. Yasuda, Y. Segawa, K. Kimoto, *J. Cryst. Growth* **1994**, *135*, 318.
[27] J. C. Bouley, P. Blanconnier, A. Herman, P. Ged, P. Henoc, J. P. Noblanc, *J. Appl. Phys.* **1976**, *46*, 3549.
[28] a) B. Hu, A. Yin, G. Karczewski, H. Luo, S. W. Short, N. Samarth, M. Dobrowolska, J. K. Furdyna, *J. Appl. Phys.* **1993**, *74*, 4153. b) M. Germaim, E. Kaetheuser, M. Soltani, O. Pages, M. Certier, W. Taudt, M. Heuken, *Phys. Status Solidi B* **1998**, *210*, 367.
[29] C. R. Wang, J. M. Hou, J. Q. Hou, Q. Li, *Jpn. J. Appl. Phys.* **2004**, *43*, 7798.
[30] Y. Tadanori, K. Masahiro, K. Motoi, N. Koji, S. Makoto, *J. Electron. Microsc.* **1995**, *44*, 488.
[31] W. I. Park, Y. H. Jun, S. W. Jung, G. C. Yi, *Appl. Phys. Lett.* **2003**, *82*, 964.

